

Bayesian phase difference estimation algorithm for direct calculation of fine structure splitting: accelerated simulation of relativistic and quantum many-body effects

Kenji Sugisaki,^{1, 2, 3,*} V. S. Prasanna,³ Satoshi Ohshima,⁴ Takahiro Katagiri,⁴ Yuji Mochizuki,^{5, 6} B. K. Sahoo,⁷ and B. P. Das^{3, 8, †}

¹*Department of Chemistry, Graduate School of Science, Osaka Metropolitan University, 3-3-138 Sugimoto, Sumiyoshi-ku, Osaka 558-8585, Japan*

²*JST PRESTO, 4-1-8 Honcho, Kawaguchi, Saitama 332-0012, Japan*

³*Centre for Quantum Engineering, Research and Education (CQuERE), TCG Centres for Research and Education in Science and Technology (TCG CREST), Sector V, Salt Lake, Kolkata 700091, India*

⁴*Information Technology Center, Nagoya University, Furo-cho, Chikusa-ku, Nagoya, Aichi 464-8601, Japan*

⁵*Department of Chemistry, Faculty of Science, Rikkyo University 3-34-1 Nishi-ikebukuro, Toshima-ku, Tokyo 171-8501, Japan*

⁶*Institute of Industrial Science, The University of Tokyo, 4-6-1 Komaba, Meguro-ku, Tokyo 153-8505, Japan*

⁷*Atomic, Molecular and Optical Physics Division,*

Physical Research Laboratory, Navrangpura, Ahmedabad 380009, India

⁸*Department of Physics, School of Science, Tokyo Institute of Technology, 2-12-1 Ookayama, Meguro-ku, Tokyo 152-8550, Japan*

(Dated: January 30, 2023)

Despite rapid progress in the development of quantum algorithms in quantum computing as well as numerical simulation methods in classical computing for atomic and molecular applications, no systematic and comprehensive electronic structure study of atomic systems that covers almost all of the elements in the periodic table using a single quantum algorithm has been reported. In this work, we address this gap by implementing the recently-proposed quantum algorithm, the Bayesian Phase Difference Estimation (BPDE) approach, to compute accurately fine-structure splittings, which are relativistic in origin and it also depends on quantum many-body (electron correlation) effects, of appropriately chosen states of atomic systems, including highly-charged superheavy ions. Our numerical simulations reveal that the BPDE algorithm, in the Dirac–Coulomb–Breit framework, can predict the fine-structure splitting of Boron-like ions to within 605.3 cm^{-1} of root mean square deviations from the experimental ones, in the (1s, 2s, 2p, 3s, 3p) active space. We performed our simulations of relativistic and electron correlation effects on Graphics Processing Unit (GPU) by utilizing NVIDIA’s cuQuantum, and observe a $\times 42.7$ speedup as compared to the CPU-only simulations in an 18-qubit active space.

I. INTRODUCTION

Quantum computing and quantum information processing are currently among the fastest growing areas of research in modern science. In particular, recent rapid progress in the development of quantum hardware such as proof-of-principle experiments of surface code quantum error correction [1–3] motivates us to anticipate fault-tolerant quantum computing (FTQC) in the future. Among the wide landscape of diverse topics in quantum computing, sophisticated ab initio electronic structure calculations of atoms and molecules on quantum computers has especially attracted much attention due to its promising real-world applications [4–6]. Aiming for practical quantum computations, proper choice of a versatile quantum algorithm that can treat both light and heavy elements in the periodic table on the same footing is of crucial importance. The total energy of an atom or

an atomic ion increases with atomic number. The variational quantum eigensolver (VQE) [7, 8] is one of the most extensively studied algorithms for quantum chemical calculations on near-term quantum devices, but its ability to predict energies of heavier systems with a sufficiently small standard deviation is limited by a massive increase in the measurement cost. In contrast, quantum phase estimation (QPE)-based approaches [9–12] are able to compute total energies of atoms and molecules with nearly constant measurement overhead regardless of the magnitude of total energies, although development of sophisticated theoretical methods to prepare approximate wave function having sufficiently large overlap with the target electronic state is necessary [13–16]. The quantum circuit for QPE is usually too deep to execute on a noisy intermediate-scale quantum (NISQ) device, but QPE is anticipated to be a powerful tool for electronic structure calculations of atoms and molecules in the FTQC era. A systematic study of the electronic structure of atoms and atomic systems with different atomic numbers entails accounting for the effects of special relativity, since the associated physical effects become prominent for the heavier elements. It is worth noting that even for the

* sugisaki@omu.ac.jp

† bhanu.das@tcgcrest.org

lighter atoms, physical phenomena that originates due to relativistic effects, such as the fine structure splitting, can be experimentally measured. However, most of the quantum simulations for quantum chemical calculations reported so far employ a non-relativistic Hamiltonian, and works in literature that take into account relativistic effects are still quite limited [17–21].

In this backdrop, we report numerical quantum simulations for the direct calculation of fine structure splitting of Boron isoelectronic sequence ($5 \leq Z \leq 103$, where Z is the atomic number of the considered system) by using a Bayesian phase difference estimation (BPDE) algorithm in conjunction with the relativistic Dirac–Coulomb–Breit Hamiltonian. Fine structure splitting is, as discussed below in detail, a purely relativistic effect and is affected by electron correlation, and therefore sophisticated treatments of both relativistic and correlation effects are necessary to calculate it quantitatively. Since experimental fine-structure splitting of wide variety of isoelectronic ions have been reported [22], it is a good testing ground for the sophisticated quantum chemical calculations on a quantum computer. The BPDE algorithm, which is recently proposed by one of the authors of the current work [23–25], is a general quantum algorithm for the direct calculation of energy gaps at the full configuration interaction (FCI) level of theory and it is suitable to compute small energy differences of systems with large total energies using a quantum computer. Accelerating the computation times for quantum simulations using state-of-the-art techniques is an extremely important factor in carrying out numerical simulations of nearly a hundred systems rapidly. In this work, we report such an acceleration by utilizing Graphics Processing Unit (GPU) with NVIDIA’s cuQuantum Software Developer Kit (SDK) [26]. To the best of our knowledge, this is the first comprehensive study of electronic structures of isoelectronic atomic series those covers almost all elements in the periodic table using a quantum algorithm.

Fine structure splitting refers to the energy separation caused by the consequence of couplings between electron spin angular momentum, S , and the orbital angular momentum L , corresponding to two atomic states with different values of the total angular momentum quantum number, J . As an example, the electronic configuration of the ground state of Boron atom ($Z = 5$) in the non-relativistic scheme is $(1s)^2(2s)^2(2p)^1$. However, in the relativistic case, the degeneracy in six p spin-orbitals is lifted and they split into two $p_{j=1/2}$ and four $p_{j=3/2}$ spin-orbitals. As a result, the electronic states ${}^2P_{1/2} = (1s_{1/2})^2(2s_{1/2})^2(2p_{1/2})^1$ and ${}^2P_{3/2} = (1s_{1/2})^2(2s_{1/2})^2(2p_{3/2})^1$ have different energies. The experimental value for the fine-structure splitting of B atom is 15.287 cm^{-1} [27], while in Boron-like Tungsten (W^{69+}), the energy gap is $1.1802 \times 10^7 \text{ cm}^{-1}$ [28] (about six orders of magnitude larger than that of B). As pointed out above, the fine structure splitting is a purely relativistic effect and is affected by electron correlation. Accurate determination of these splittings would therefore serve as

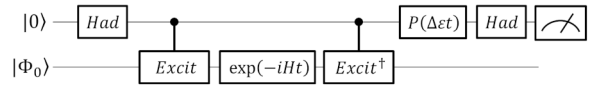


FIG. 1. Quantum circuit for the BPDE algorithm.

sensitive tests of relativistic many-electron theories [29–35]. The extent to which the fine structure splitting is affected by electron correlation depends on the choice of system as well as the chosen states [29, 36]. In the case of boron isoelectronic sequence, the correlation effects reduce in importance as we go from lighter to heavier ions, while for our choice of states for these systems (${}^2P_{1/2}$ and ${}^2P_{3/2}$), pair correlation effects are the most important. In particular, the two particle-two hole excitations that result in configurations such as $(1s_{1/2})^2(2p_{1/2})^1(2p_{3/2})^2$, $(1s_{1/2})^2(2p_{1/2})^2(2p_{3/2})^1$, and $(1s_{1/2})^2(2p_{3/2})^3$ are dominant. From the view point of quantum computation, a careful choice of systems such that their fine-structure splittings span six orders of magnitude, followed by accurate determination of these quantities by a suitable quantum algorithm (BPDE in this case) would be a testament to the versatility of that algorithm.

II. THEORY

A typical quantum circuit for the BPDE algorithm is illustrated in Fig. 1. Here, we have used the notation ‘Had’ for the Hadamard gate to distinguish it from the Hamiltonian, H . $P(\Delta\varepsilon t)$ is a phase rotation gate defined as

$$P(\Delta\varepsilon t) = \begin{pmatrix} 1 & 0 \\ 0 & e^{i\Delta\varepsilon t} \end{pmatrix}, \quad (1)$$

where $\Delta\varepsilon$ is used as the estimator of the energy gap. $|\Phi_0\rangle$ is an approximated wave function for the ground state. An approximated excited state wave function $|\Phi_1\rangle$ is generated by applying an *Excit* gate to $|\Phi_0\rangle$. These approximated wave functions can be expanded in the basis of eigenfunctions $\{|\Psi_j\rangle\}$ as

$$|\Phi_0\rangle = \sum_j c_j |\Psi_j\rangle \quad (2)$$

and

$$|\Phi_1\rangle = \sum_k d_k |\Psi_k\rangle. \quad (3)$$

Using Eqs (2) and (3), the probability of measuring the $|0\rangle$ state, $Prob(0)$, in the quantum circuit depicted in Fig 1 is calculated as

$$Prob(0) = \frac{1}{2} \left[1 + \sum_{j,k} |c_j|^2 |d_k|^2 \cos\{(\Delta E_{jk} - \Delta\varepsilon)t\} \right] \quad (4)$$

From Eq (4), if the approximated wave functions have sufficiently large overlap with the eigenfunction of corresponding target states, $\text{Prob}(0)$ becomes maximum around the point where $\Delta\varepsilon$ equals the energy difference between the two targeted states. Thus, we can calculate the energy gap by finding that value of $\Delta\varepsilon$ that gives maximum $\text{Prob}(0)$. In the BPDE algorithm, $\Delta\varepsilon$ is optimized by means of Bayesian inference in the following procedure. (I) Define a prior distribution $\text{Pr}(\Delta\varepsilon)$ by a Gaussian function, in which the mean, μ , corresponds to an initial estimate of the energy gap with a standard deviation σ . Note that σ determines the energy range of the Bayesian search, and it should be large enough so that true ΔE locates between $(\mu - \sigma)$ and $(\mu + \sigma)$. (II) Repeatedly execute the quantum circuit in Fig 1 with a fixed evolution time $t = 1.8/\sigma$ and different $\Delta\varepsilon$ in the range between $(\mu - \sigma)$ and $(\mu + \sigma)$ and generate the $\Delta\varepsilon$ vs. $\text{Prob}(0)$ plot. Then, the plot is fitted by a Gaussian function and is used as a likelihood function $\text{Pr}(0|\Delta\varepsilon; t)$. (III) Calculate a posterior distribution $\text{Pr}(\Delta\varepsilon|0; t)$ using the equation

$$\text{Pr}(\Delta\varepsilon|0; t) = \frac{\text{Pr}(0|\Delta\varepsilon; t)\text{Pr}(\Delta\varepsilon)}{\int \text{Pr}(0|\Delta\varepsilon; t)\text{Pr}(\Delta\varepsilon)d(\Delta\varepsilon)}. \quad (5)$$

Since both $\text{Pr}(0|\Delta\varepsilon; t)$ and $\text{Pr}(\Delta\varepsilon)$ are given as Gaussian functions, we can easily compute the posterior distribution. (IV) If the standard deviation of $\text{Pr}(\Delta\varepsilon|0; t)$ is smaller than the convergence threshold E_{Thre} , then return the mean of $\text{Pr}(\Delta\varepsilon|0; t)$ as the estimate of ΔE . Otherwise return to step (II) using the posterior distribution as the prior distribution in the next iteration.

The time evolution of wave functions is implemented using conventional techniques as follows. The second-quantized electronic Hamiltonian, built out of creation and annihilation operators (denoted below by a^\dagger and a respectively, and with their indices running over the chosen single particle basis), is given by

$$H = \sum_{pq} h_{pq} a_p^\dagger a_q + \frac{1}{2} \sum_{pqrs} h_{pqrs} a_p^\dagger a_q^\dagger a_s a_r \quad (6)$$

and is transformed to a qubit Hamiltonian, which then takes the form

$$H = \sum_j w_j (\sigma_{N-1} \otimes \sigma_{N-2} \otimes \cdots \otimes \sigma_0), \sigma \in \{I, X, Y, Z\} \quad (7)$$

using the Jordan–Wigner transformation [37]. In the equations (6) and (7), h_{pq} and h_{pqrs} refer to the one- and two-electron integrals, while in the qubit Hamiltonian, w_j refers to the pre-factors for each of the terms in the transformed Hamiltonian, with each w_j being a product of either a one- or a two-electron integral and a multiplicative factor resulting from the transformation itself. Subsequently, the quantum circuit corresponding

to the time evolution operators is constructed [38] using second-order Trotter–Suzuki decomposition [39–41].

In the present study, we tested two different Hamiltonians: H_{DC} and $H_{\text{DC+B}}$. H_{DC} is the Dirac–Coulomb Hamiltonian, defined by the equation (in atomic units)

$$H_{\text{DC}} = \sum_i [c\boldsymbol{\alpha}_i \cdot \mathbf{p}_i + (\beta_i - 1)c^2 + V_n(r_i)] + \sum_{j>i} \frac{1}{r_{ij}} \quad (8)$$

while $H_{\text{DC+B}}$ contains an additional term, V_{B} , given by

$$V_{\text{B}} = - \sum_{j>i} \left\{ \frac{\boldsymbol{\alpha}_i \cdot \boldsymbol{\alpha}_j}{2r_{ij}} + \frac{(\boldsymbol{\alpha}_i \cdot \mathbf{r}_{ij})(\boldsymbol{\alpha}_j \cdot \mathbf{r}_{ij})}{2r_{ij}^3} \right\} \quad (9)$$

to take into account the full Breit interaction in addition to H_{DC} . In the above equations, c is the speed of light, $\boldsymbol{\alpha}$ and β are the 4×4 Dirac matrices, \mathbf{p}_i is the momentum operator associated with the i^{th} electron, $V_n(r_i)$ is the electron–nucleus potential, and $1/r_{ij}$ is the electron–electron Coulomb interaction term. A recent theoretical study by Wan and coworkers showed that relative contributions of Breit interactions to the fine-structure splitting of B isoelectronic sequence are significant for light elements, and is as large as 14.55% for neutral Boron [35].

For the accurate computation of fine-structure splitting, it is important to treat the ${}^2P_{1/2}$ ground state and the ${}^2P_{3/2}$ excited state on an equal footing [29]. In this work, the one- and two-electron integrals were computed at the Dirac–Fock level for the state with one electron removed from the corresponding target systems (B^+ and its isoelectronic sequence) using our own in-house code. Gaussian-type universal basis ($\alpha_0 = 0.01$ and $\beta = 1.80$) with 40 $s_{1/2}$, 39 $p_{1/2}$, and 39 $p_{3/2}$ orbitals is used for the Dirac–Fock calculations. The large and the small components of Dirac–Fock orbitals are kinetically balanced [42]. In the BPDE simulations, we tested two types of active spaces; (1s, 2s, 2p) with 10 qubits and (1s, 2s, 2p, 3s, 3p) with 18 qubits, without adopting any qubit tapering techniques. Note that two-qubit tapering based on electron number conservation rule in the parity basis and the symmetry-conserving Bravyi–Kitaev transformation [43] assumes non-relativistic calculations in which the electron spin quantum number is a good quantum number. Applying these techniques to relativistic calculations is not straightforward. Throughout this paper, when we use, for example, the notation $(18q, H_{\text{DC+B}})$, it specifies the active space and Hamiltonian being used.

We now comment on the effect of Trotter error on our results. It is known that Trotter decomposition error depends on the maximum atomic charge of a system [44], and therefore finer Trotter decomposition should be employed for heavier elements. In the present study, we set the time length of a single Trotter step as $t/M = \max[0.2, |h_{00}|]$, where M is the number of Trotter slices and h_{00} is the one-electron integral corresponding to electron–nuclear attraction of the $1s_{1/2}$

electrons. We used single Slater determinant wave functions for the approximated wave functions of the $^2P_{1/2}$ and the $^2P_{3/2}$ states: $|\Phi_0\rangle = |(1s_{1/2})^2(2s_{1/2})^2(2p_{1/2})^1\rangle$ and $|\Phi_1\rangle = |(1s_{1/2})^2(2s_{1/2})^2(2p_{3/2})^1\rangle$, respectively. In this case, the controlled-*Excit* gate in Fig 1 is realized by two CNOT gates. The difference between the energy expectation values of two approximated wave functions is used as the initial mean of the prior distribution: $\mu_{ini} = \Delta E_{Ref} = \langle\Phi_1|H|\Phi_1\rangle - \langle\Phi_0|H|\Phi_0\rangle$, and the initial standard deviation of the prior distribution is set as $\sigma_{ini} = \max[0.1, 10|\mu_{ini}|]$ in units of Hartree. In step (II) of the BPDE algorithm, we draw 21 samples in the range of $(\mu - \sigma)$ to $(\mu + \sigma)$ with a constant interval, and execute the quantum circuit 5,000 times for each sample to construct the likelihood function. The convergence threshold for Bayesian optimization in the step (IV) is set to be inversely proportional to the time of a single Trotter step, $E_{Thre} = 0.001M/t$ Hartree. These computational conditions were selected to calculate the fine-structure splitting of Boron isoelectronic sequence with similar computational costs regardless of the atomic number Z . Using these conditions, the number of Trotter slices, M , in the final iteration is about 1,000 for all atoms being studied.

The numerical simulation program for the BPDE algorithm was developed using Python3 with OpenFermion[45], Cirq[46], and cuQuantum[26] libraries. To execute numerical simulations with GPU acceleration, we prepared the simulation environment on a Supercomputer “Flow” Type II subsystem in Nagoya University. The “Flow” Type II subsystem consists of the FUJITSU Server PRIMERGY CX2570 M5, including the Intel Xeon Gold 6230 with 20 cores \times 2 sockets, and the NVIDIA Tesla V100 (Volta) \times 4 GPUs, thus 33.888 TFLOPS in a node. 384 GiB (DDR4 2933 MHz) memory, and 6.4TB/node SSD in each node are available. In addition, local shared storage (BeeGFS, BeeOND, NVMe) is also provided. The total number of nodes is 221, and hence total FLOPS is $33.888 \text{ TFLOPS} \times 221 \text{ nodes} = 7.489 \text{ PFLOPS}$. The numerical simulations for 10 qubit active space were executed on Linux workstations without GPU accelerations, and those for 18 qubit active space were carried out on “Flow” Type II subsystem. Because the BPDE algorithm computes the likelihood function based on statistical sampling of the measurement outcome, the algorithm returns different values for every run. In this study, all the numerical simulations were carried out five times. The standard deviations of five runs for B are about 0.7–2.0 cm $^{-1}$, and those for Boron-like ions (99 atoms in total) are on average 199.8, 163.2, 136.3, and 167.7 cm $^{-1}$ for $(10q, H_{DC})$, $(18q, H_{DC})$, $(10q, H_{DC+B})$, and $(18q, H_{DC+B})$, respectively, and they are sufficiently small compared to the calculated values of ΔE_{BPDE} .

III. RESULTS AND DISCUSSION

The fine-structure splitting values obtained from the numerical simulations of the BPDE algorithm using $(18q, H_{DC+B})$ as well as the experimental values [22] are plotted in Fig 2(a), and the ratios $\Delta E_{BPDE}/\Delta E_{Exptl}$ and $\Delta E_{BPDE}/\Delta E_{CASCI}$ are given in Fig 2(b) and (c), re-

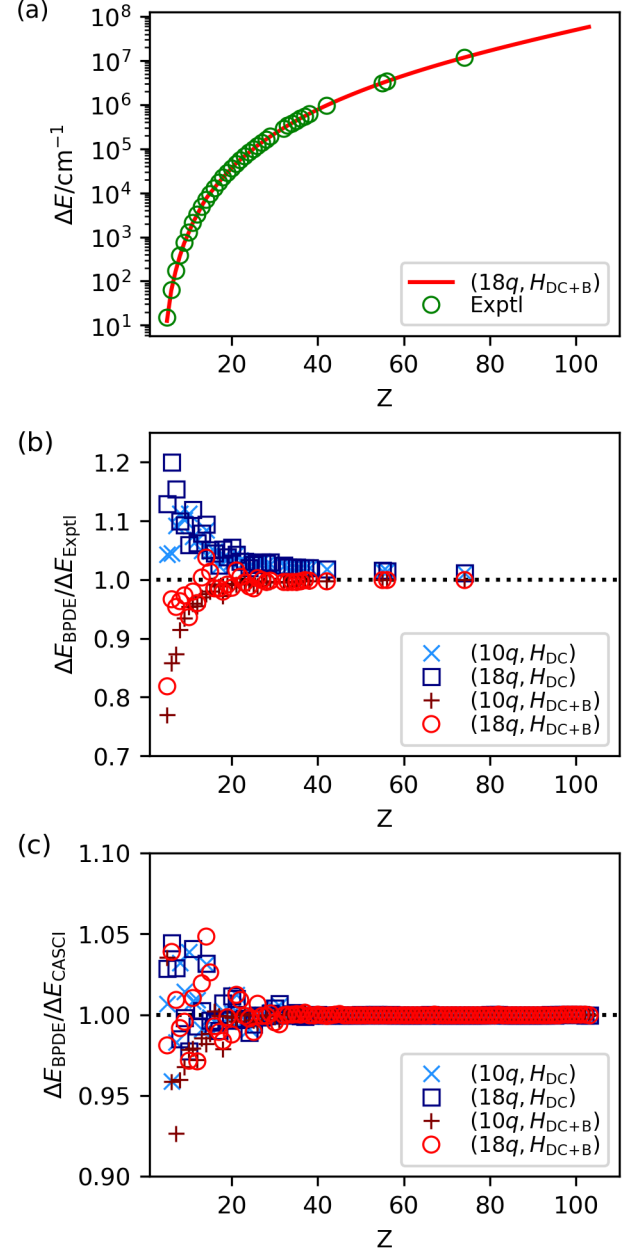


FIG. 2. Results of numerical simulations of the BPDE-based fine-structure splitting calculations. (a) The fine-structure splitting values calculated by the BPDE algorithm using $(18q, H_{DC+B})$ (red line) and experimental values (green circles). (b) The $\Delta E_{BPDE}/\Delta E_{Exptl}$ values. (c) The $\Delta E_{BPDE}/\Delta E_{CASCI}$ values.

spectively. Note that CASCI is the acronym for complete active space configuration interaction, and it corresponds to the FCI treatment within the selected active orbitals. All the calculated fine-structure splitting values are provided in the Supplemental Material. For light elements, deviation of the ΔE_{BPDE} values from experimental ones appears to be large, but this observation is a consequence of the fine-structure splitting being small. In fact, the fine-structure splitting of B calculated using the BPDE algorithm with (18q, $H_{\text{DC}+\text{B}}$) is $\Delta E = 12.5287 \pm 0.9813 \text{ cm}^{-1}$, and the absolute error with respect to the experimental value is only about 3 cm^{-1} . Note that the ΔE value of B calculated at the CASCI level is 12.2715 cm^{-1} and therefore departure of the ΔE_{BPDE} value from the experimental one is well explained by the limited active space size. Note that all the $\Delta E_{\text{BPDE}}/\Delta E_{\text{CASCI}}$ values (Fig 2c) are in the range 0.92 and 1.05, thus indicating the ability of the BPDE algorithm in being able to reproduce the CASCI fine-structure splitting very accurately. We expect that inclusion of more virtual orbitals (3d, 4s, 4p, and above) can further improve the accuracy of the fine-structure splitting. The agreement in the values of ΔE_{BPDE} with ΔE_{Exptl} in highly charged ions is also worth emphasizing. In this context, we note that for heavier ions, relativistic effects are dominant and electron correlation effects becomes less significant. Nevertheless, the fine-structure splittings computed by using the BPDE algorithm are closer to the experimental values than those estimated from the reference wave functions ΔE_{Ref} . For example, the fine-structure splitting in Boron-like Tungsten (W^{69+}) is calculated to be $\Delta E_{\text{Ref}} = 11,841,730 \text{ cm}^{-1}$ and $\Delta E_{\text{BPDE}} = 11,800,183 \text{ cm}^{-1}$ for (18q, $H_{\text{DC}+\text{B}}$), and the experimental value is $\Delta E_{\text{Exptl}} = 11,802,000 \text{ cm}^{-1}$. These results also exemplify the capability of the BPDE algorithm in predicting the energy gap accurately. The root mean square deviations of the ΔE_{BPDE} from ΔE_{Exptl} were calculated as 9966.6, 10139.7, 698.0, and 605.3 cm^{-1} for (10q, H_{DC}), (18q, H_{DC}), (10q, $H_{\text{DC}+\text{B}}$), and (18q, $H_{\text{DC}+\text{B}}$), respectively. It is worth noting that the larger active space with more sophisticated Hamiltonian (18q, $H_{\text{DC}+\text{B}}$) gives the best agreement with the experimental values.

In order to check for GPU acceleration in our numerical quantum circuit simulation, we executed the BPDE calculations of Boron fine-structure splitting with 8, 10, 16, and 18 qubit active spaces in conjunction with $H_{\text{DC}+\text{B}}$ on our Linux workstation (CPU: Intel Xeon-Gold 6134, GPU: None) and “Flow” Type II subsystem (CPU: Intel Xeon-Gold 6230, GPU: NVIDIA Tesla V100). The 8 and 16 qubit active spaces were prepared by fixing the occupation number of $1s_{1/2}$ orbitals in the 10 and 18 qubit active spaces, respectively. For 8 and 10 qubit active spaces, we also carried out the BPDE simulations on “Flow” Type II subsystem without using GPU. All the simulations were performed five times using single thread.

The average simulation time of five runs are given in

TABLE I. Average time taken for BPDE quantum circuit simulation for B atom fine-structure splitting, in units of seconds.

Size of active space	Workstation ^a	“Flow”	Type II ^b
	w/o GPU	w/o GPU	with GPU
8	628	731	177
10	2197	2267	588
16	73452	—	4830
18	387328	—	9081

^a CPU: Intel Xeon-Gold 6134, GPU: None

^b CPU: Intel Xeon-Gold 6230, GPU: NVIDIA Tesla V100

Table I. From the table, the speedup in GPU-accelerated quantum circuit simulations is significant, especially when a larger active space is employed. For smaller active spaces (8q and 10q), the speedup is about $\times 4$. By contrast, for 16 and 18 qubit active spaces, GPU-based simulations provide substantial speedups of 15.2 and 42.7 times, respectively. Note that the computation times of both CPU and GPU-based quantum circuit simulations scales exponentially with the number of qubits, but the exponent is smaller for GPU than CPU.

IV. SUMMARY

In summary, our numerical quantum simulations reveal that quantum computers have the potential of computing fine-structure splitting of Boron isoelectronic sequence very accurately by appropriately considering both relativistic and quantum many-body effects using the Bayesian phase difference estimation algorithm. By using the (1s, 2s, 2p, 3s, 3p) active space and the relativistic Dirac–Coulomb–Breit Hamiltonian, the fine-structure splittings in Boron isoelectronic sequence were predicted within 605.3 cm^{-1} of the root mean square deviation from the experimental values. This root mean square deviation value is the smallest among the four cases involving different combinations of Hamiltonian and number of qubits that we tested. It is noteworthy that the deviations in the calculated fine structure splittings from the experimental values do not increase nearly as much as they do with increase in atomic number. Two of our important findings in this work regarding accuracy of the calculated fine structure splitting are (a) that it is crucial to include Breit interactions for accurate predictions of fine-structure splittings for the systems that we have considered, and (b) that it is necessary to include virtual orbitals to improve our results for the lighter systems (neutral Boron and the lighter Boron-like ions). Speedup in numerical simulations of quantum circuits by using GPU in conjunction with NVIDIA cuQuantum is significant, especially when large active space is employed. We observed $\times 42.7$ speedup for 18-qubit active space simulations. Such acceleration of quantum circuit simulations is important to test the ability of the quantum algorithms

to handle problems of larger size, for further development of quantum algorithms for various applications.

ACKNOWLEDGMENTS

The authors thank Shinya Morino (NVIDIA Japan) for helpful discussions on the cuQuantum simulation en-

vironment construction on “Flow” Type II subsystem. This work was supported by JST PRESTO “Quantum Software” project (Grant No. JPMJPR1914), Japan and KAKENHI Scientific Research C (Grant No. 21K03407) from JSPS, Japan. The computation was carried out using the JHPCN Joint Research Projects (jh220010) on supercomputer “Flow” at Information Technology Center, Nagoya University.

-
- [1] S. Krinner, N. Lacroix, A. Remm, A. Di Paolo, E. Genois, C. Leroux, C. Hellings, S. Lazar, F. Swiadek, J. Herrmann, G. J. Norris, C. K. Andersen, M. Müller, A. Blais, C. Eichler, and A. Wallraff. Realizing repeated quantum error correction in a distance-three surface code. *Nature*, 605:669–674, 2022.
- [2] Y. Zhao, Y. Ye, H. L. Huang, Y. Zhang, D. Wu, and H. Guan *et al.* Realization of an error-correcting surface code with superconducting qubits. *Phys. Rev. Lett.*, 129:030501, 2022.
- [3] R. Acharya *et al.* Suppressing quantum errors by scaling a surface code logical qubit. arXiv:2207.06431, 2022.
- [4] Y. Cao, J. Romero, J. P. Olson, M. Degroote, P. D. Johnson, M. Kieferová, I. D. Kivlichan, T. Menke, B. Peropadre, N. P. D. Sawaya, S. Sim, L. Veis, and A. Aspuru-Guzik. Quantum chemistry in the age of quantum computing. *Chem. Rev.*, 119:10856–10915, 2019.
- [5] B. Bauer, S. Bravyi, M. Motta, and G. K.-L. Chan. Quantum algorithms for quantum chemistry and quantum materials science. *Chem. Rev.*, 120:12685–12717, 2020.
- [6] M. Motta and J. E. Rice. Emerging quantum computing algorithms for quantum chemistry. *WIREs Comput. Mol. Sci.*, 12:e1580, 2022.
- [7] A. Peruzzo, J. McClean, P. Shadbolt, M.-H. Yung, X.-Q. Zhou, P. J. Love, A. Aspuru-Guzik, and J. L. O’Brien. A variational eigenvalue solver on a photonic quantum processor. *Nat. Comm.*, 5:4213, 2014.
- [8] J. Tilly, H. Chen, S. Cao, D. Picozzi, K. Setia, Y. Li, E. Grant, L. Wossnig, I. Rungger, G. H. Booth, and J. Tennyson. The variational quantum eigensolver: a review of methods and best practices. *Phys. Rep.*, 986:1–128, 2022.
- [9] A. Aspuru-Guzik, A. D. Dutoi, P. J. Love, and M. Head-Gordon. Simulated quantum computation of molecular energies. *Science*, 309:1704–1707, 2005.
- [10] B. P. Lanyon, J. D. Whitfield, G. G. Gillett, M. E. Goggin, M. P. Almeida, I. Kassal, J. D. Biamonte, M. Mohseni, B. J. Powell, M. Barbieri, A. Aspuru-Guzik, and A. G. White. Towards quantum chemistry on a quantum computer. *Nat. Chem.*, 2:106–111, 2010.
- [11] J. Du, N. Xu, X. Peng, P. Wang, S. Wu, and D. Lu. NMR implementation of a molecular hydrogen quantum simulation with adiabatic state preparation. *Phys. Rev. Lett.*, 104:030502, 2010.
- [12] N. P. Bauman, H. Liu, E. J. Bylaska, S. Krishnamoorthy, G. H. Low, C. E. Granade, N. Wiebe, N. A. Baker, B. Peng, M. Roetteler, M. Troyer, and K. Kowalski. Toward quantum computing for high-energy excited states in molecular systems: quantum phase estimations of core-level states. *J. Chem. Theory Comput.*, 17:201–210, 2021.
- [13] L. Veis and J. Pittner. Adiabatic state preparation study of methylene. *J. Chem. Phys.*, 140:214111, 2014.
- [14] K. Sugisaki, S. Nakazawa, K. Toyota, K. Sato, D. Shiomi, and T. Takui. Quantum chemistry on quantum computers: a method for preparation of multiconfigurational wave functions on quantum computers without performing post-Hartree–Fock calculations. *ACS Cent. Sci.*, 5:167–175, 2019.
- [15] K. Sugisaki, K. Toyota, K. Sato, D. Shiomi, and T. Takui. Adiabatic state preparation of correlated wave functions with nonlinear scheduling functions and broken-symmetry wave functions. *Comm. Chem.*, 5:84, 2022.
- [16] D. Halder, V. S. Prasanna, V. Agarawal, and R. Maitra. Iterative quantum phase estimation with variationally prepared reference state. *Int. J. Quantum Chem.*, page e27021, 2022.
- [17] L. Veis, J. Višňák, T. Fleig, S. Knecht, T. Saue, L. Visscher, and J. Pittner. Relativistic quantum chemistry on quantum computers. *Phys. Rev. A*, 85:030304(R), 2012.
- [18] V. A. Zaytsev, M. E. Groshev, I. A. Maltsev, A. V. Durova, and V. M. Shabaev. Calculation of the moscovium ground-state energy by quantum algorithms. arXiv:2207.08255, 2022.
- [19] T. F. Stetina, A. Ciavarella, X. Li, and N. Wiebe. Simulating effective QED on quantum computers. *Quantum*, 6:622, 2022.
- [20] K. R. Swain, V. S. Prasanna, K. Sugisaki, and B. P. Das. Calculation of molecular electric dipole moments of light and moderately heavy molecules using relativistic VQE algorithm. arXiv:2211.06907, 2022.
- [21] V. Kumar, N. Baskaran, V. S. Prasanna, K. Sugisaki, D. Mukherjee, K. G. Dyall, and B. P. Das. Accurate calculation of relativistic excitation energies using quantum annealing. arXiv:2212.01801, 2022.
- [22] NIST atomic spectra database levels data. https://physics.nist.gov/PhysRefData/ASD/levels_form.html. Retrieved: 2022-08-22.
- [23] K. Sugisaki, C. Sakai, K. Toyota, K. Sato, D. Shiomi, and T. Takui. Bayesian phase difference estimation: a general quantum algorithm for the direct calculation of energy gaps. *Phys. Chem. Chem. Phys.*, 23:20152–20162, 2021.
- [24] K. Sugisaki, C. Sakai, K. Toyota, K. Sato, D. Shiomi, and T. Takui. Quantum algorithm for full configuration interaction calculations without controlled time evolutions. *J. Phys. Chem. Lett.*, 12:11085–11089, 2021.
- [25] K. Sugisaki, H. Wakimoto, K. Toyota, K. Sato, D. Shiomi, and T. Takui. Quantum algorithm for numerical energy gradient calculations at the full configuration interaction level of theory. *J. Phys. Chem. Lett.*, 13:11105–2021.

- 11111, 2022.
- [26] NVIDIA cuQuantum team. NVIDIA/cuQuantum: cuQuantum v22.05.0.
- [27] A. E. Kraminda and A. N. Ryabtsev. A critical compilation of energy levels and spectral lines of neutral boron. *Phys. Scr.*, 76:544–557, 2007.
- [28] J. Clementson, P. Beiersdorfer, G. V. Brown, M. F. Gu, H. Lundberg, Y. Podpaly, and E. Träbert. Tungsten spectroscopy at the Livermore electron beam ion trap facility. *Can. J. Phys.*, 89:571–580, 2011.
- [29] B. P. Das, J. Hata, and I. P. Grant. Ground-state fine structure in the boron isoelectronic sequence. *J. Phys. B: At. Mol. Phys.*, 17:L1–L5, 1984.
- [30] B. P. Das, K. V. P. Latha, B. K. Sahoo, C. Sur, R. K. Chaudhuri, and D. Mukherjee. Relativistic and correlation effects in atoms. *J. Theor. Comp. Chem.*, 4:1–20, 2005.
- [31] J. P. Marques, P. Indelicato, and F. Parente. Relativistic multiconfiguration calculations of the $2s^22p\ ^2P_{3/2}$ level lifetime along the boron isoelectronic sequence. *Eur. Phys. J. D*, 66:324, 2012.
- [32] N. N. Dutta and S. Majumder. *Ab initio* studies of electron correlation and Gaunt interaction effects in the boron isoelectronic sequence using coupled-cluster theory. *Phys. Rev. A*, 85:032512, 2012.
- [33] A. N. Artemyev, V. M. Shabaev, I. I. Tupitsyn, G. Plunien, A. Surzhykov, and S. Fritzsch. *Ab initio* calculations of the $2p_{3/2} - 2p_{1/2}$ fine-structure splitting in boron-like ions. *Phys. Rev. A*, 88:032518, 2013.
- [34] Y. Yu and B. K. Sahoo. Investigating ground-state fine-structure properties to explore suitability of boronlike $S^{11+} - K^{14+}$ and galliumlike $Nb^{10+} - Ru^{13+}$ ions as possible atomic clocks. *Phys. Rev. A*, 99:022513, 2019.
- [35] J.-J. Wan, J. Li, and J. Gu. Residual electronic correlation and QED effects in fine-structure splitting of ground configuration for the boron isoelectronic sequence. *Result Phys.*, 31:105004, 2021.
- [36] W. F. Perger and B. P. Das. Multiconfigurational Dirac-Fock calculations of fine-structure intervals in the beryllium isoelectronic sequence. *J. Phys. B: At. Mol. Phys.*, 20:665, 1987.
- [37] P. Jordan and E. Wigner. Über das Paulische äquivalenzverbot. *Z. Phys.*, 47:631–651, 1928.
- [38] J. D. Whitfield, J. Biamonte, and A. Aspuru-Guzik. Simulation of electronic structure Hamiltonians using quantum computers. *Mol. Phys.*, 109:735–750, 2011.
- [39] H. F. Trotter. On the product of semi-groups of operators. *Proc. Am. Math. Soc.*, 10:545–551, 1959.
- [40] M. Suzuki. Relationship between d -dimensional quantal spin systems and $(d + 1)$ -dimensional Ising systems: equivalence, critical exponents and systematic approximants of the partition function and spin correlations. *Prog. Theor. Phys.*, 56:1454–1469, 1976.
- [41] N. Hatano and M. Suzuki. Finding exponential product formulas of higher orders. In A. Das and B. K. Chakrabarti, editors, *Quantum Annealing and Other Optimization Methods, Lecture Notes in Physics*, volume 679, pages 37–68. Springer, New York, 2005.
- [42] K. G. Dyall, I. P. Grant, and S. Wilson. The dirac equation in the algebraic approximation. ii. extended basis set calculations for hydrogenic atoms. *J. Phys. B*, 17:L45, 1984.
- [43] S. Bravyi, J. M. Gambetta, A. Mezzacapo, and K. Temme. Tapering off qubits to simulate fermionic Hamiltonians. arXiv:1701.08213, 2017.
- [44] R. Babbush, J. McClean, D. Wecker, A. Aspuru-Guzik, and N. Wiebe. Chemical basis of Trotter-Suzuki errors in quantum chemistry simulation. *Phys. Rev. A*, 91:022311, 2015.
- [45] J. R. McClean *et al.* OpenFermion: the electronic structure package for quantum computers. *Quantum Sci. Technol.*, 5:034014, 2020.
- [46] Cirq developers. Cirq, version v1.0.0. <https://github.com/quantumlib/Cirq>.

SUPPLEMENTAL MATERIAL

TABLE S1. Fine structure splitting of Boron isoelectronic sequence calculated using H_{DC} .

Atom	ΔE_{Ref}	$\Delta E_{\text{CASCI}(10q)}$	$\Delta E_{\text{BPDE}(10q)}$	$\Delta E_{\text{CASCI}(18q)}$	$\Delta E_{\text{BPDE}(18q)}$	$\Delta E_{\text{Exptl}}^{\text{a}}$
B	17.9174	15.8486	15.9481 \pm 1.2618	16.7709	17.2684 \pm 1.9425	15.287
C ⁺	74.868	69.831	66.296 \pm 1.574	71.989	76.088 \pm 6.982	63.42
N ²⁺	202.79	192.26	190.42 \pm 0.98	195.97	201.23 \pm 2.98	174.4
O ³⁺	442.28	422.50	429.59 \pm 9.91	428.09	424.54 \pm 6.25	385.9
F ⁴⁺	842.74	808.52	820.26 \pm 2.66	816.38	813.68 \pm 5.11	744.5
Ne ⁵⁺	1456.56	1407.02	1455.09 \pm 32.58	1417.54	1384.46 \pm 4.05	1306.81
Na ⁶⁺	2368.89	2283.50	2292.26 \pm 37.54	2297.12	2390.01 \pm 4.71	2134.61
Mg ⁷⁺	3638.30	3512.34	3528.87 \pm 51.17	3529.50	3508.24 \pm 7.99	3302
Al ⁸⁺	5356.23	5176.92	5132.37 \pm 23.11	5198.09	5276.66 \pm 49.49	4890
Si ⁹⁺	7617.46	7369.72	7582.29 \pm 281.69	7395.39	7647.06 \pm 28.88	6990.6
P ¹⁰⁺	10526.07	10192.46	10175.27 \pm 5.90	10223.13	10192.56 \pm 7.21	9699
S ¹¹⁺	14195.56	13756.22	13781.11 \pm 139.22	13792.41	13734.39 \pm 120.46	13135.3
Cl ¹²⁺	18749.02	18181.61	17827.99 \pm 32.46	18223.86	17842.14 \pm 88.91	17410
Ar ¹³⁺	24319.18	23598.96	23508.34 \pm 260.68	23647.82	23843.43 \pm 141.14	22656.239
K ¹⁴⁺	31048.63	30148.47	30036.00 \pm 103.44	30204.49	30149.39 \pm 95.46	29017
Ca ¹⁵⁺	39089.90	37980.39	37647.62 \pm 301.63	38044.15	38530.65 \pm 280.51	36520
Sc ¹⁶⁺	48605.67	47255.28	47680.40 \pm 877.20	47327.35	47617.66 \pm 314.80	45637
Ti ¹⁷⁺	59768.90	58144.16	58117.48 \pm 145.09	58225.12	58024.71 \pm 51.44	56240
V ¹⁸⁺	72763.06	70828.77	70739.20 \pm 157.39	70919.22	70751.88 \pm 77.13	68610
Cr ¹⁹⁺	87782.29	85501.81	84842.85 \pm 442.65	85602.32	84460.94 \pm 212.75	82970
Mn ²⁰⁺	105032	102367	101745 \pm 220	102478	101935 \pm 481	99360
Fe ²¹⁺	124727	121640	121629 \pm 18	121762	121769 \pm 69	118266
Co ²²⁺	147097	143548	143592 \pm 54	143682	143428 \pm 138	139290
Ni ²³⁺	172379	168329	168364 \pm 301	168475	168480 \pm 159	163960
Cu ²⁴⁺	200825	196234	196465 \pm 77	196394	197027 \pm 196	191280
Zn ²⁵⁺	232698	227528	228371 \pm 964	227701	228747 \pm 310	
Ga ²⁶⁺	268274	262486	263850 \pm 592	262673	264403 \pm 35	
Ge ²⁷⁺	307841	301399	301484 \pm 262	301600	301747 \pm 223	294550
As ²⁸⁺	351700	344568	344740 \pm 249	344784	344750 \pm 96	337400
Se ²⁹⁺	400166	392311	392679 \pm 81	392543	392775 \pm 61	384460
Br ³⁰⁺	453569	444958	445279 \pm 373	445206	445945 \pm 42	436400
Kr ³¹⁺	512250	502853	502510 \pm 453	503117	502733 \pm 668	492560
Rb ³²⁺	576568	566358	565943 \pm 269	566639	566283 \pm 431	554700
Sr ³³⁺	652881	635846	635884 \pm 182	636144	636082 \pm 204	623100
Y ³⁴⁺	723619	711707	711912 \pm 113	712023	711874 \pm 141	
Zr ³⁵⁺	807144	794349	794633 \pm 35	794683	794833 \pm 122	
Nb ³⁶⁺	897891	884195	883919 \pm 151	884547	884216 \pm 69	
Mo ³⁷⁺	996297	981684	981773 \pm 145	982055	981726 \pm 559	964360
Tc ³⁸⁺	1102818	1087273	1087296 \pm 427	1087664	1087542 \pm 275	
Ru ³⁹⁺	1217926	1201440	1201283 \pm 284	1201850	1201776 \pm 291	
Rh ⁴⁰⁺	1342115	1324677	1324715 \pm 100	1325107	1325094 \pm 122	
Pd ⁴¹⁺	1475895	1457498	1457410 \pm 220	1457949	1457916 \pm 230	
Ag ⁴²⁺	1619798	1600438	1600596 \pm 254	1600910	1600721 \pm 86	
Cd ⁴³⁺	1774377	1754051	1754295 \pm 91	1754543	1754580 \pm 225	
In ⁴⁴⁺	1940207	1918912	1918639 \pm 115	1919427	1919129 \pm 29	
Sn ⁴⁵⁺	2117884	2095621	2096259 \pm 90	2096158	2096422 \pm 129	
Sb ⁴⁶⁺	2308028	2284799	2284125 \pm 143	2285359	2284924 \pm 176	
Te ⁴⁷⁺	2511283	2487091	2487548 \pm 194	2487673	2487648 \pm 135	
I ⁴⁸⁺	2728321	2703171	2703597 \pm 192	2703777	2704096 \pm 141	
Xe ⁴⁹⁺	2959835	2933731	2934128 \pm 196	2934362	2934422 \pm 197	
Cs ⁵⁰⁺	3206549	3179500	3179630 \pm 128	3180155	3180328 \pm 166	3131500
Ba ⁵¹⁺	3469213	3441225	3440903 \pm 52	3441905	3441680 \pm 197	3390000
La ⁵²⁺	3748611	3719693	3719951 \pm 86	3720399	3720606 \pm 163	
Ce ⁵³⁺	4045553	4015715	4015654 \pm 116	4016448	4016555 \pm 158	
Pr ⁵⁴⁺	4360884	4330136	4330527 \pm 193	4330896	4331133 \pm 123	
Nd ⁵⁵⁺	4695479	4663830	4663813 \pm 139	4664619	4664367 \pm 140	

^a NIST Atomic spectra database levels data. https://physics.nist.gov/PhysRefData/ASD/levels_form.html. Retrieved: 2022-08-22.

Atom	ΔE_{Ref}	$\Delta E_{\text{CASCI}(10q)}$	$\Delta E_{\text{BPDE}(10q)}$	$\Delta E_{\text{CASCI}(18q)}$	$\Delta E_{\text{BPDE}(18q)}$	$\Delta E_{\text{Exptl}}^{\text{a}}$
Pm ⁵⁶⁺	5050254	5017718	5017925 \pm 305	5018534	5018126 \pm 137	
Sm ⁵⁷⁺	5426153	5392737	5393112 \pm 208	5393583	5393480 \pm 235	
Eu ⁵⁸⁺	5824171	5789889	5789980 \pm 52	5790766	5790877 \pm 124	
Gd ⁵⁹⁺	6245328	6210189	6210225 \pm 405	6211097	6211030 \pm 57	
Tb ⁶⁰⁺	6690696	6654722	6654865 \pm 169	6655662	6655651 \pm 360	
Dy ⁶¹⁺	7161401	7124590	7126185 \pm 212	7125563	7126567 \pm 75	
Ho ⁶²⁺	7658589	7620961	7620883 \pm 202	7621967	7621731 \pm 111	
Er ⁶³⁺	8183474	8145040	8145092 \pm 530	8146081	8145938 \pm 238	
Tm ⁶⁴⁺	8737316	8698090	8697909 \pm 279	8699168	8698577 \pm 226	
Yb ⁶⁵⁺	9321420	9281411	9281615 \pm 161	9282526	9282366 \pm 53	
Lu ⁶⁶⁺	9937169	9896391	9896412 \pm 258	9897545	9897147 \pm 157	
Hf ⁶⁷⁺	10585979	10544442	10543803 \pm 123	10545635	10544828 \pm 179	
Ta ⁶⁸⁺	11269350	11227067	11226933 \pm 418	11228302	11228238 \pm 42	
W ⁶⁹⁺	11988832	11945815	11945395 \pm 227	11947092	11946340 \pm 65	11802000
Re ⁷⁰⁺	12746058	12702317	12702908 \pm 91	12703638	12703808 \pm 86	
Os ⁷¹⁺	13542712	13498254	13498082 \pm 240	13499621	13498828 \pm 266	
Ir ⁷²⁺	14380594	14335433	14336439 \pm 189	14336847	14337502 \pm 63	
Pt ⁷³⁺	15261542	15215686	15215990 \pm 198	15217149	15217012 \pm 125	
Au ⁷⁴⁺	16187517	16140977	16141619 \pm 228	16142490	16142679 \pm 39	
Hg ⁷⁵⁺	17160527	17113306	17115189 \pm 231	17114872	17116484 \pm 347	
Tl ⁷⁶⁺	18182718	18134822	18136036 \pm 139	18136442	18137391 \pm 180	
Pb ⁷⁷⁺	19256340	19207778	19209871 \pm 306	19209454	19212153 \pm 54	
Bi ⁷⁸⁺	20383744	20334524	20334279 \pm 175	20336259	20335669 \pm 296	
Po ⁷⁹⁺	21567411	21517545	21517352 \pm 149	21519341	21517098 \pm 554	
At ⁸⁰⁺	22809881	22759368	22758762 \pm 167	22761228	22760323 \pm 135	
Rn ⁸¹⁺	24113621	24062411	24061957 \pm 95	24064337	24063545 \pm 183	
Fr ⁸²⁺	25481984	25430126	25430910 \pm 243	25432121	25432069 \pm 350	
Ra ⁸³⁺	26917680	26865161	26864880 \pm 96	26867227	26865772 \pm 189	
Ac ⁸⁴⁺	28423992	28370819	28371577 \pm 241	28372960	28372993 \pm 133	
Th ⁸⁵⁺	30004040	29950180	29950357 \pm 110	29952399	29952000 \pm 235	
Pa ⁸⁶⁺	31661735	31607219	31607974 \pm 131	31609518	31610122 \pm 266	
U ⁸⁷⁺	33400172	33344927	33346253 \pm 169	33347312	33348148 \pm 220	
Np ⁸⁸⁺	35224049	35168122	35169013 \pm 183	35170595	35170749 \pm 94	
Pu ⁸⁹⁺	37136625	37079925	37082405 \pm 135	37082491	37084472 \pm 152	
Am ⁹⁰⁺	39143289	39085864	39087449 \pm 79	39088526	39090163 \pm 129	
Cm ⁹¹⁺	41247805	41189575	41192822 \pm 335	41192338	41194995 \pm 84	
Bk ⁹²⁺	43455815	43396788	43400513 \pm 83	43399657	43403286 \pm 249	
Cf ⁹³⁺	45771812	45711897	457115583 \pm 412	45714877	45718006 \pm 232	
Es ⁹⁴⁺	48202067	48141250	48147673 \pm 39	48144347	48150157 \pm 168	
Fm ⁹⁵⁺	50751624	50689785	50696869 \pm 408	50693004	50699333 \pm 89	
Md ⁹⁶⁺	53427857	53364982	53373015 \pm 471	53368330	53375378 \pm 204	
No ⁹⁷⁺	56236972	56172980	56172549 \pm 383	56176463	56175545 \pm 145	
Lr ⁹⁸⁺	59185705	59120454	59120944 \pm 44	59124080	59123626 \pm 337	

^a NIST Atomic spectra database levels data. https://physics.nist.gov/PhysRefData/ASD/levels_form.html. Retrieved: 2022-08-22.

TABLE S2. Fine structure splitting of Boron isoelectronic sequence calculated using H_{DC+B} .

Atom	ΔE_{Ref}	$\Delta E_{\text{CASCI}(10q)}$	$\Delta E_{\text{BPDE}(10q)}$	$\Delta E_{\text{CASCI}(18q)}$	$\Delta E_{\text{BPDE}(18q)}$	$\Delta E_{\text{Exptl}}^{\text{a}}$
B	13.1978	11.5561	11.7684 \pm 0.7139	12.2715	12.5287 \pm 0.9813	15.287
C ⁺	60.457	56.316	54.401 \pm 2.097	58.092	61.322 \pm 1.553	63.42
N ²⁺	171.73	162.92	152.35 \pm 4.14	166.03	166.34 \pm 4.94	174.4
O ³⁺	385.83	369.04	353.09 \pm 0.24	373.80	371.88 \pm 3.26	385.9
F ⁴⁺	750.43	720.98	695.63 \pm 7.23	727.72	725.22 \pm 1.89	744.5
Ne ⁵⁺	1322.09	1273.76	1246.66 \pm 4.82	1282.83	1223.61 \pm 1.60	1306.81
Na ⁶⁺	2166.36	2091.18	2047.99 \pm 3.12	2102.97	2092.85 \pm 5.20	2134.61
Mg ⁷⁺	3357.84	3245.90	3152.15 \pm 3.90	3260.83	3171.26 \pm 3.70	3302
Al ⁸⁺	4980.23	4819.58	4743.64 \pm 59.12	4838.05	4907.62 \pm 83.88	4890
Si ⁹⁺	7126.46	6902.91	6819.95 \pm 49.83	6925.39	7255.91 \pm 47.77	6990.6
P ¹⁰⁺	9898.75	9595.83	9505.88 \pm 42.88	9622.77	9835.82 \pm 70.06	9699
S ¹¹⁺	13408.75	13007.61	13036.97 \pm 14.92	13039.49	12949.81 \pm 51.71	13135.3
Cl ¹²⁺	17777.63	17257.01	17223.49 \pm 61.68	17294.32	17153.48 \pm 439.42	17410
Ar ¹³⁺	23136.18	22472.44	22021.84 \pm 70.65	22515.70	22210.14 \pm 148.62	22656.239
K ¹⁴⁺	29625.02	28792.19	28760.39 \pm 7.72	28841.92	28794.81 \pm 38.32	29017
Ca ¹⁵⁺	37394.68	36364.54	36255.11 \pm 16.97	36421.27	36026.58 \pm 275.92	36520
Sc ¹⁶⁺	46605.79	45348.01	45273.12 \pm 208.58	45412.29	46394.58 \pm 324.34	45637
Ti ¹⁷⁺	57429.26	55911.57	55957.54 \pm 20.84	55983.94	56506.46 \pm 410.85	56240
V ¹⁸⁺	70046.41	68234.83	68225.92 \pm 37.58	68315.84	68274.12 \pm 15.36	68610
Cr ¹⁹⁺	84649.24	82508.32	82487.91 \pm 166.57	82598.53	82016.14 \pm 389.31	82970
Mn ²⁰⁺	101441	98934	98606 \pm 28	99034	97952 \pm 85	99360
Fe ²¹⁺	120634	117724	117064 \pm 122	117834	118606 \pm 71	118266
Co ²²⁺	142456	139103	138991 \pm 61	139225	139282 \pm 296	139290
Ni ²³⁺	167141	163309	163205 \pm 16	163442	163367 \pm 69	163960
Cu ²⁴⁺	194940	190589	190574 \pm 129	190734	190942 \pm 246	191280
Zn ²⁵⁺	226112	221205	220977 \pm 5	221362	220323 \pm 90	
Ga ²⁶⁺	260931	255430	254797 \pm 57	255600	254113 \pm 133	
Ge ²⁷⁺	299681	293551	293579 \pm 25	293735	293665 \pm 75	294550
As ²⁸⁺	342663	335869	335815 \pm 40	336066	336175 \pm 190	337400
Se ²⁹⁺	390189	382696	383035 \pm 66	382907	383035 \pm 129	384460
Br ³⁰⁺	442583	434360	434336 \pm 148	434587	434744 \pm 462	436400
Kr ³¹⁺	500186	491204	491490 \pm 44	491446	491550 \pm 121	492560
Rb ³²⁺	563353	553584	554126 \pm 15	553841	554563 \pm 297	554700
Sr ³³⁺	632452	621871	621906 \pm 67	622144	622050 \pm 93	623100
Y ³⁴⁺	707870	696452	696249 \pm 142	696742	696679 \pm 152	
Zr ³⁵⁺	790006	777731	777783 \pm 149	778038	778127 \pm 68	
Nb ³⁶⁺	879278	866128	865827 \pm 99	866452	866419 \pm 104	
Mo ³⁷⁺	976119	962077	962423 \pm 56	962419	962080 \pm 70	964360
Tc ³⁸⁺	1080982	1066034	1065869 \pm 56	1066394	1066314 \pm 123	
Ru ³⁹⁺	1194336	1178469	1179121 \pm 102	1178848	1179323 \pm 108	
Rh ⁴⁰⁺	1316669	1299874	1300951 \pm 109	1300272	1301248 \pm 238	
Pd ⁴¹⁺	1448489	1430757	1430699 \pm 193	1431174	1431057 \pm 238	
Ag ⁴²⁺	1590323	1571649	1571393 \pm 40	1572086	1571904 \pm 121	
Cd ⁴³⁺	1742720	1723099	1723176 \pm 154	1723556	1723573 \pm 53	
In ⁴⁴⁺	1906249	1885679	1885323 \pm 134	1886157	1885771 \pm 21	
Sn ⁴⁵⁺	2081503	2059983	2059583 \pm 102	2060482	2060263 \pm 25	
Sb ⁴⁶⁺	2269097	2246627	2247118 \pm 218	2247148	2247141 \pm 278	
Te ⁴⁷⁺	2469670	2446251	2446077 \pm 54	2446794	2446222 \pm 57	
I ⁴⁸⁺	2683888	2659525	2658861 \pm 212	2660091	2659622 \pm 84	
Xe ⁴⁹⁺	2912439	2887135	2886491 \pm 113	2887723	2887212 \pm 54	
Cs ⁵⁰⁺	3156042	3129802	3129582 \pm 81	3130415	3129932 \pm 230	3131500
Ba ⁵¹⁺	3415441	3388271	3387950 \pm 117	3388908	3388588 \pm 39	3390000
La ⁵²⁺	3691414	3663321	3663278 \pm 131	3663983	3663899 \pm 64	
Ce ⁵³⁺	3984765	3955756	3955821 \pm 192	3956444	3956279 \pm 98	
Pr ⁵⁴⁺	4296331	4266416	4266307 \pm 270	4267129	4267222 \pm 177	
Nd ⁵⁵⁺	4626983	4596167	4595512 \pm 80	4596907	4596254 \pm 31	

^a NIST Atomic spectra database levels data. https://physics.nist.gov/PhysRefData/ASD/levels_form.html. Retrieved: 2022-08-22.

Atom	ΔE_{Ref}	$\Delta E_{\text{CASCI}(10q)}$	$\Delta E_{\text{BPDE}(10q)}$	$\Delta E_{\text{CASCI}(18q)}$	$\Delta E_{\text{BPDE}(18q)}$	$\Delta E_{\text{Exptl}}^{\text{a}}$
Pm ⁵⁶⁺	4977628	4945922	4946187 ± 80	4946690	4946621 ± 317	
Sm ⁵⁷⁺	5349202	5316613	5316863 ± 373	5317410	5317433 ± 123	
Eu ⁵⁸⁺	5742695	5709234	5709494 ± 100	5710060	5710148 ± 174	
Gd ⁵⁹⁺	6159116	6124790	6125085 ± 238	6125647	6125513 ± 52	
Tb ⁶⁰⁺	6599537	6564358	6564535 ± 36	6565246	6565470 ± 183	
Dy ⁶¹⁺	7065057	7029033	7028710 ± 55	7029953	7029302 ± 128	
Ho ⁶²⁺	7556830	7519972	7521113 ± 240	7520925	7521955 ± 128	
Er ⁶³⁺	8076055	8038372	8038164 ± 72	8039359	8038847 ± 143	
Tm ⁶⁴⁺	8623983	8585485	8584963 ± 248	8586508	8585682 ± 49	
Yb ⁶⁵⁺	9201907	9162601	9161613 ± 148	9163661	9162670 ± 20	
Lu ⁶⁶⁺	9811201	9771098	9770656 ± 278	9772195	9771630 ± 335	
Hf ⁶⁷⁺	10453268	10412375	10411155 ± 149	10413511	10412464 ± 36	
Ta ⁶⁸⁺	11129599	11087924	11087367 ± 88	11089101	11088670 ± 132	
W ⁶⁹⁺	11841730	11799282	11799251 ± 162	11800500	11800183 ± 44	11802000
Re ⁷⁰⁺	12591280	12548066	12547901 ± 101	12549328	12548956 ± 240	
Os ⁷¹⁺	13379921	13335944	13335230 ± 210	13337251	13336476 ± 286	
Ir ⁷²⁺	14209438	14164708	14164993 ± 58	14166062	14166361 ± 304	
Pt ⁷³⁺	15081655	15036176	15035743 ± 98	15037578	15037037 ± 200	
Au ⁷⁴⁺	15998517	15952295	15953120 ± 154	15953747	15954372 ± 204	
Hg ⁷⁵⁺	16962015	16915050	16915529 ± 362	16916554	16917045 ± 191	
Tl ⁷⁶⁺	17974279	17926571	17926948 ± 293	17928130	17928614 ± 331	
Pb ⁷⁷⁺	19037539	18989093	18991354 ± 337	18990708	18992455 ± 296	
Bi ⁷⁸⁺	20154128	20104947	20104226 ± 124	20106621	20105993 ± 162	
Po ⁷⁹⁺	21326506	21276597	21275126 ± 30	21278332	21276994 ± 167	
At ⁸⁰⁺	22557193	22506550	22505988 ± 225	22508348	22507537 ± 188	
Rn ⁸¹⁺	23848636	23797206	23796693 ± 79	23799071	23798543 ± 206	
Fr ⁸²⁺	25204159	25151982	25150246 ± 234	25153915	25152050 ± 135	
Ra ⁸³⁺	26626449	26573508	26573283 ± 306	26575513	26575312 ± 86	
Ac ⁸⁴⁺	28118763	28065058	28063868 ± 255	28067138	28065659 ± 174	
Th ⁸⁵⁺	29684193	29629687	29629591 ± 486	29631846	29632012 ± 173	
Pa ⁸⁶⁺	31326619	31271332	31270575 ± 84	31273573	31272033 ± 194	
U ⁸⁷⁺	33049108	32992968	32993309 ± 235	32995294	32995444 ± 129	
Np ⁸⁸⁺	34856318	34799359	34799070 ± 47	34801774	34801172 ± 66	
Pu ⁸⁹⁺	36751482	36693612	36694673 ± 199	36696121	36697077 ± 376	
Am ⁹⁰⁺	38739941	38681195	38682438 ± 173	38683802	38684875 ± 340	
Cm ⁹¹⁺	40825427	40765721	40766742 ± 492	40768431	40769554 ± 410	
Bk ⁹²⁺	43013532	42952865	42955744 ± 173	42955682	42958575 ± 432	
Cf ⁹³⁺	45308712	45246987	45249757 ± 288	45249918	45252590 ± 142	
Es ⁹⁴⁺	47717180	47654374	47658797 ± 346	47657424	47661160 ± 340	
Fm ⁹⁵⁺	50243937	50179928	50186129 ± 423	50183103	50188868 ± 103	
Md ⁹⁶⁺	52896291	52831053	52837308 ± 182	52834360	52841209 ± 105	
No ⁹⁷⁺	55680394	55613837	55622434 ± 394	55617282	55624337 ± 436	
Lr ⁹⁸⁺	58602919	58534900	58533663 ± 431	58538491	58536631 ± 617	

^a NIST Atomic spectra database levels data. https://physics.nist.gov/PhysRefData/ASD/levels_form.html. Retrieved: 2022-08-22.